

## Parallel electric fields are inefficient drivers of energetic electrons in magnetic reconnection

J. T. Dahlin,<sup>1, a)</sup> J. F. Drake,<sup>1, b)</sup> and M. Swisdak<sup>1</sup>

*Institute for Research in Electronics and Applied Physics,  
University of Maryland, College Park, Maryland 20742,  
USA*

We present two-dimensional kinetic simulations, with a broad range of initial guide fields, that isolate the role of parallel electric fields ( $E_{\parallel}$ ) in energetic electron production during collisionless magnetic reconnection. In the strong guide field regime,  $E_{\parallel}$  drives essentially all of the electron energy gain, yet fails to generate an energetic component. We suggest that this is due to the weak energy scaling of particle acceleration from  $E_{\parallel}$  compared to that of a Fermi-type mechanism responsible for energetic electron production in the weak guide-field regime. This result has important implications for energetic electron production in astrophysical systems and reconnection-driven dissipation in turbulence.

PACS numbers: 52.35.Vd, 94.30.cp, 52.65.Rr, 96.60.Iv

---

<sup>a)</sup>jdahlin@umd.edu; Jack Eddy Postdoctoral Fellow; Heliophysics Science Division, NASA Goddard Space Flight Center, Greenbelt, MD 20771, USA

<sup>b)</sup>Department of Physics, University of Maryland, College Park, Maryland 20742, USA; Institute for Physical Science and Technology, University of Maryland, College Park, Maryland 20742, USA

Magnetic fields are significant reservoirs of energy in many plasmas. Magnetic reconnection converts that energy into other forms, principally the thermal and kinetic energy of the surrounding particles. Of particular interest in many systems is the production of non-thermal particles with energies much larger than typical of the ambient medium. Among the phenomena in which such energetic particle production occurs are gamma-ray bursts<sup>1,2</sup>, stellar and solar flares<sup>3</sup>, and magnetospheric storms<sup>4</sup>. Observations of solar flares, in particular, demonstrate that the acceleration can be particularly efficient: a large fraction of the electrons in the flaring region become non-thermal<sup>5,6</sup>. The energy content of this population is comparable to that of the initial magnetic field.

The mechanisms by which reconnection can foster particle acceleration are a topic of significant interest e.g.<sup>7-13</sup>. Two specific processes have received the most attention. The first is acceleration by electric fields parallel to the local magnetic field ( $E_{\parallel}$ )<sup>9,14,15</sup>. However, the number of electrons that can be accelerated through this mechanism may be limited because during magnetic reconnection non-zero  $E_{\parallel}$  typically only occur near X-lines and separatrices.

In the second process<sup>16</sup>, charged particles gain energy as they reflect from the ends of contracting magnetic islands. (An analogous process occurs during the acceleration of cosmic rays by the first-order Fermi mechanism.) In contrast to the localization of  $E_{\parallel}$ , this can occur wherever there are contracting field lines, including the merging of magnetic islands in the outflows of single X-line reconnection<sup>12,13,16-18</sup> and in turbulent reconnecting systems where magnetic field lines are stochastic and conventional islands do not exist<sup>19</sup>. This mechanism is therefore volume-filling and can accelerate a large number of particles.

A recent article<sup>20</sup> developed a method for calculating electron acceleration due to both of these mechanisms as well as betatron acceleration associated with conservation of the magnetic moment. This study found that Fermi reflection dominates in reconnection where the magnetic fields are roughly antiparallel (see also<sup>21,22</sup>), whereas in guide field reconnection both Fermi reflection and  $E_{\parallel}$  are important drivers of particle energization. In another study, Numata et al.<sup>23</sup> found that  $E_{\parallel}$  drove electron heating in a gyrokinetic system corresponding to an asymptotically strong guide field, and Wang<sup>24</sup> found a similar result in a system with a guide field twice that of the reconnecting component. In another article<sup>19</sup>, we showed that the Fermi mechanism, which scales like  $v_{\parallel}^2$  compared with  $v_{\parallel}$  for  $E_{\parallel}$ , was the dominant accelerator of energetic electrons in a system with a guide field equal to the reconnecting

component, even though both mechanisms were equal contributors to the overall electron energy gain.

In this article, we explore electron heating over the full range of guide fields, from much smaller to much larger than the reconnecting field. We find that Fermi reflection is the dominant mechanism in reconnection with a weak guide field, whereas  $E_{\parallel}$  drives essentially all of the electron energization in the strong guide field regime. We present simple models for each mechanism that reveal the essential physics behind the guide field scaling. Most significantly we show that energetic electron production is strongly suppressed in the strong guide field regime where the parallel electric field dominates electron energy gain, suggesting more generally that parallel electric fields are not efficient drivers of energetic particles in nature.

In order to examine electron energization we assume a guiding-center approximation relevant for a strong guide field<sup>19,25</sup>. In this limit, the evolution of the kinetic energy  $\epsilon = (\gamma - 1)m_e c^2$  of a single electron can be written as:

$$\frac{d\epsilon}{dt} = qE_{\parallel}v_{\parallel} + \frac{\mu}{\gamma} \left( \frac{\partial B}{\partial t} + \mathbf{u}_E \cdot \nabla B \right) + \gamma m_e v_{\parallel}^2 (\mathbf{u}_E \cdot \boldsymbol{\kappa}) \quad (1)$$

where  $E_{\parallel} = \mathbf{E} \cdot \mathbf{b}$  is the parallel electric field,  $\mu = m_e \gamma^2 v_{\perp}^2 / 2B$  is the magnetic moment,  $\mathbf{u}_E = c\mathbf{E} \times \mathbf{B} / B^2$ , and  $\boldsymbol{\kappa} = \mathbf{b} \cdot \nabla \mathbf{b}$  is the magnetic curvature. The velocity components parallel and perpendicular to the magnetic field are  $v_{\parallel}$  and  $v_{\perp}$ , respectively;  $\gamma$  is the relativistic Lorentz factor, and  $\mathbf{b}$  is the unit vector in the direction of the local magnetic field.

The first term on the right-hand-side of the equation corresponds to acceleration by a parallel electric field, which is typically localized near the reconnection X-line and along separatrices. The second term corresponds to betatron acceleration associated with  $\mu$  conservation in a temporally and spatially varying magnetic field. Because reconnection releases a system's magnetic energy, this typically causes electron cooling<sup>20</sup>. The last term corresponds to Fermi reflection of particles from contracting magnetic field lines<sup>13,16,17,20</sup>. Both  $E_{\parallel}$  and Fermi reflection change the parallel energy of the particles, while betatron acceleration changes the perpendicular energy. The term  $\mathbf{u}_E \cdot \boldsymbol{\kappa}$  corresponds to a local field-line contraction:  $\mathbf{u}_E \cdot \boldsymbol{\kappa} = -\dot{\ell}/\ell$  (where  $\ell$  is the field-line length) and is linked to the conservation of the parallel adiabatic invariant  $J_{\parallel} = \int v_{\parallel} d\ell$ <sup>16,17</sup>. The guide-field approximation given in Eq. (1) is accurate when electrons are well-magnetized. In the weak-guide field regime, other terms such as the polarization drift may be significant (compare Li et al.<sup>22</sup>). However, the

polarization drift gives the change in the electron bulk flow energy which is typically small for a physical mass ratio.

It is informative to compare Eq. 1 to the evolution of the magnetic energy:

$$\frac{\partial B^2}{\partial t} \frac{1}{8\pi} + \nabla \cdot \mathbf{S} = -\mathbf{E} \cdot \mathbf{J} \quad (2)$$

where  $\mathbf{S} = c\mathbf{E} \times \mathbf{B}/4\pi$  is the Poynting flux and the displacement current has been neglected in Ampère's law. The current  $\mathbf{J}$  may be separated into parallel and perpendicular components so that Eq. (2) becomes:

$$\frac{\partial B^2}{\partial t} \frac{1}{8\pi} + \nabla \cdot \left( \frac{B^2}{4\pi} \mathbf{u}_E \right) = -E_{\parallel} J_{\parallel} - \mathbf{E} \cdot \left[ \frac{c\mathbf{B}}{B^2} \times \left( \frac{\mathbf{B} \cdot \nabla \mathbf{B}}{4\pi} - \frac{\nabla B^2}{8\pi} \right) \right] \quad (3)$$

This equation may be rearranged into the following useful form:

$$\frac{\partial B^2}{\partial t} \frac{1}{8\pi} + \nabla \cdot \left( \frac{B^2}{8\pi} \mathbf{u}_E \right) = -E_{\parallel} J_{\parallel} - \frac{B^2}{8\pi} \nabla \cdot \mathbf{u}_E - (\mathbf{u}_E \cdot \boldsymbol{\kappa}) \frac{B^2}{4\pi} \quad (4)$$

The second term on the left-hand side is the divergence of magnetic energy flux, which vanishes in a volume-integration. The first term on the right-hand side has a clear analogue in the  $E_{\parallel}$  term in Eq. (1). The third term corresponds to the mechanical work done by the magnetic tension force ( $\boldsymbol{\kappa}B^2/4\pi$ ). This term contains the field-line contraction  $\mathbf{u}_E \cdot \boldsymbol{\kappa}$  and is therefore related to the Fermi reflection term in Eq. (1). Beresnyak and Li<sup>26</sup> have also noted the link between energy conversion via the tension force and first-order Fermi acceleration via the curvature drift. The  $\nabla \cdot \mathbf{u}_E$  term describes the change in magnetic energy associated with compression or expansion.

We explore particle acceleration in reconnection via simulations using the particle-in-cell (PIC) code `p3d`<sup>27</sup>. Particle trajectories are calculated using the relativistic Newton-Lorentz equation, and the electromagnetic fields are advanced using Maxwell's equations. The time and space coordinates are normalized, respectively, to the proton cyclotron frequency based on the reconnecting magnetic field  $\Omega_{ci}^{-1} = m_i c / e B_{x0}$  and the proton inertial length  $d_i = c / \omega_{pi}$ . The typical grid cell width is  $\Delta = d_e / 8$  where  $d_e = d_i \sqrt{m_e / m_i}$  is the electron inertial length, and the time step is  $dt = \Omega_{ci}^{-1} / 200 = \Omega_{ce}^{-1} / 8$ , where  $\Omega_{ce} = (m_i / m_e) \Omega_{ci}$  is the electron cyclotron frequency. The domain size is  $51.2d_i \times 25.6d_i$ , and we vary the guide field  $b_g \equiv B_{z0} / B_{x0} \in [0, 0.2, 0.5, 1.0, 2.0, 4.0]$ . For  $b_g = 4.0$ ,  $\Delta = d_e / 16$  and  $dt = \Omega_{ci} / 400$ . In terms of electron Larmor radius,  $\Delta / \rho_e \in [0.177, 0.180, 0.198, 0.25, 0.395, 0.364]$ .

We use an artificial proton-to-electron mass ratio  $m_i / m_e = 25$  to reduce the computational expense. All simulations use at least 200 particles per cell. The initial electron and

proton temperatures are isotropic, with  $T_e = T_i = 0.25m_i c_A^2$ , and the initial density  $n_0$  and pressure  $p$  are constant so that  $\beta_x = 8\pi p/B_{x0}^2 = 0.5$ . The speed of light is  $c = 3c_A\sqrt{m_i/m_e}$ , where  $c_A = B_0/\sqrt{4\pi m_i n_0}$  is the Alfvén speed based on the reconnecting component of the magnetic field.

All simulations are initialized with a force-free configuration and use periodic boundary conditions. This is chosen as the most generic model for large-scale systems such as the solar corona where the density jump between the current layer and upstream plasma is not expected to be important. The magnetic field is given by  $B_x = B_{x0} \tanh(y/w_0)$  and  $B_z = \sqrt{(1 + b_g^2)B_{x0}^2 - B_x^2}$ , corresponding to an asymptotic guide field  $B_{z0} = b_g B_{x0}$ . We include two current sheets at  $y = L_y/4$  and  $3L_y/4$  to produce a periodic system, and  $w_0 = 1.25d_e$ . This initial configuration is not a kinetic equilibrium, which would require a temperature anisotropy<sup>28</sup>, but is in pressure balance.

Reconnection begins from noise via the tearing instability, generating magnetic islands which grow and merge. Reconnection evolves nonlinearly until we halt the simulations before the two current sheets significantly interact. Panels (a-c) of Figure 1 show the cumulative electron energy gain due to the three mechanisms in Eq. (1). Bulk electron heating is calculated via the methods discussed in an earlier work<sup>20</sup>. In all cases the terms given in Eq. (1), indicated by the dashed black line, adequately capture the total energy gain of the electrons (solid black line). The difference is due to several small terms, such as the polarization drift, that were omitted from this equation.

In the weak guide field case (Fig. 1a), the largest terms are Fermi reflection (positive) and betatron acceleration (negative) which partially cancel to produce most of the electron energy gain. The contribution of parallel electric fields is negligible. The betatron term is larger than in the previous study (Dahlin et al.<sup>20</sup>) because it scales proportionally with the plasma  $\beta$ , which is significantly larger here ( $\sim 1$  vs.  $\sim 0.2$ ). In the simulation with  $b_g = 4$  (Fig. 1c), all terms but  $E_{\parallel}$  have negligible contributions to electron energy gain, a result similar to Wang et al., 2016<sup>24</sup>. In the intermediate case  $b_g = 1$ , both Fermi reflection and  $E_{\parallel}$  are important, as was reported in<sup>20</sup>. Note that the total electron energy gain is about  $\sim 50\%$  larger in the  $b_g = 0.2$  case than in the  $b_g = 4.0$  case. As  $b_g$  increases the system becomes less compressible, the consequences of which are discussed further below. Figure 2 shows the late-time spatial distribution of electron heating in simulations with  $b_g = 0.2, 4.0$ . Although the location of the heating is similar for both cases, the magnitude changes with

Fermi reflection decreasing by around a factor of 50. The energization due to Fermi and  $E_{\parallel}$  (normalized to the total electron energy gain) is shown versus the guide field in Fig. 1d. The Fermi term is greater than unity for small  $b_g$  due to the large cancellation with the betatron term. It is clear that the contribution of Fermi reflection falls off rapidly with increasing guide field, and vice-versa for  $E_{\parallel}$ .

Given the dramatic change in the mechanisms driving electron acceleration with increasing guide field, it is informative to also explore how magnetic energy is being released during the same transition. In Fig. 3 we show the time dependence of the spatially integrated rates of magnetic energy release for the three terms on the RHS of Eq. 3. For weak guide field ( $b_g = 0.2$ ) the dominant terms are from field-line expansion and magnetic tension with the contribution from  $E_{\parallel}$  being small. For larger guide fields (1.0 and 4.0) the curvature and  $E_{\parallel}$  terms are comparable and the compression term is negligible – the guide field clearly suppresses compression. Since electron energization from Fermi reflection is so weak at high guide field, the continued importance of magnetic tension in releasing magnetic energy might be surprising. However, it is well known that the outflow exhaust velocity remains at  $c_A$  even when  $b_g$  is large<sup>29</sup> so the ion bulk flow carries much of the magnetic energy released.

Fermi acceleration is driven by the reflection of a charged particle from a field line expelled by the exhaust with a velocity  $c_A$ , where  $c_A$  is the Alfvén velocity based on the reconnecting component. The energy gain due to a single reflection is given by:

$$\Delta\epsilon \approx 2mc_A \mathbf{x} \cdot v_{\parallel} \mathbf{b} = 2mv_{\parallel} c_A \frac{B_x}{B}$$

The time between reflections is:

$$\Delta t \sim L/v_x \sim LB/(v_{\parallel} B_x)$$

where  $L$  is the characteristic island length. This yields an energization rate<sup>16</sup>:

$$\dot{\epsilon} \sim mv_{\parallel}^2 \frac{2c_A}{L} \frac{B_x^2}{B^2} \propto \frac{1}{1 + B_z^2/B_x^2} \quad (5)$$

Thus, in the strong guide field regime  $B_z \gg B_x$  the scaling is  $\dot{\epsilon} \propto b_g^{-2}$ . Only the component of the electron parallel velocity along the direction of contracting magnetic field contributes to energy gain so there is less energy gain per reflection. Additionally, the time between reflections is greater in the large guide-field limit because the reflection frequency is proportional to the in-plane velocity  $v_x \sim v_{\parallel}/b_g$ . The diminished efficiency of Fermi reflection can also

be seen in the scaling of the magnetic curvature  $\kappa \sim (\mathbf{B} \cdot \nabla \mathbf{B})/B^2 \propto B_x B_y / \delta B^2 \propto B_x^2 / \delta B^2$ , where  $\delta$  is the characteristic width of the exhaust and  $B_y/B_x \sim 0.1$  is linked to the aspect ratio of the diffusion region. In the strong guide field regime, the reconnected field lines are elongated in the out-of-plane direction so that advection in the  $x - y$  plane does little to change their overall length. In the weak guide field regime,  $B \approx B_x$  and Eq. 5 is independent of  $B_z/B_x$ . The curve  $\sim [1 + 4b_g^2]^{-1}$  (solid red line in Fig. 1) describes the scaling of the heating from Fermi reflection very well (the factor of 4 yields the best fit).

In an earlier study<sup>20</sup>, we showed that the electron energy gain due to  $E_{\parallel} J_{\parallel}$  occurs around the diffusion region near the X-line (the positive and negative values in the blotchy patches distributed along separatrices and in the islands in Fig. 2 do not drive net heating). Within the diffusion region where the plasma is not frozen-in, the reconnection electric field and out-of plane current drive the energy conversion:

$$E_{\parallel} J_{\parallel} \sim \frac{J_z B_z}{B} \frac{E_z B_z}{B} \quad (6)$$

In the weak guide-field limit this term is only significant in the region where  $B_z / \sqrt{B_x^2 + B_y^2} > 1$ . The area where this inequality is satisfied is given by  $b_g^2 \delta_x \delta_y$ , where  $\delta_x$  and  $\delta_y$  are the scale lengths of  $B_y$  and  $B_x$  in the  $x$  and  $y$  directions, respectively. Thus, the fraction of the diffusion region where  $J_{\parallel} E_{\parallel}$  is significant scales as  $b_g^2$  in the weak guide field regime  $b_g \ll 1$ . This simplified description neglects important antiparallel dynamics (such as the Hall fields and meandering particle orbits) and does not completely match the simulation results, which are more consistent with  $b_g^3$ , but serves to illustrate the scaling of  $E_{\parallel}$  heating with increasing guide field. When the guide field is large ( $b_g \gtrsim 1$ ), the diffusion region is defined as the region where  $E_{\parallel}$  is non-zero and drives  $J_{\parallel}$ . In this limit, the entire diffusion region contributes to dissipation through  $J_{\parallel} E_{\parallel}$ .

Energy spectra at late time  $\Omega_{ci} t = 75$  (Fig. 4a) reveal that the production of energetic electrons in reconnection with strong guide fields is nearly completely eliminated. The normalized spectra (Fig. 4b) showcase the enhancement in energetic electrons, given by  $f_e(\epsilon, t = 75)/f_e(\epsilon, t = 0)$ . There is a substantial enhancement (a factor of  $\sim 50$ ) at  $\epsilon = 0.6 m_e c^2$  for the systems with  $b_g < 1$ , whereas for the system with  $b_g = 4$  the enhancement is  $< 2$ , and is approximately independent of  $\epsilon$  for  $\epsilon > 0.2$ . Note that in these simulations, the contribution of the energetic population to the total energy is small, so that the overall conversion of magnetic to electron energy is only weakly dependent on the guide field (see

Fig. 1a-c).

Panel (c) shows the energetic electron enhancement at  $\epsilon = 0.6$  versus the electron heating fraction due to  $E_{\parallel}$  (the same quantity is shown in Fig. 1d). It is clear that energetic electron production diminishes rapidly as the  $E_{\parallel}$  contribution increases. According to Eq. (1), energy gain from  $E_{\parallel}$  is a weaker function of energy ( $\sim v_{\parallel}$ ) than that due to the Fermi mechanism ( $\sim v_{\parallel}^2$ ). Whereas the Fermi mechanism preferentially accelerates energetic particles to generate a nonthermal tail, parallel electric fields distribute energy more evenly and drive bulk heating. This result suggests that parallel electric fields are, in general, inefficient drivers of energetic electrons.

These results have broad implications for electron energization and heating in reconnecting systems where the reconnecting component of the magnetic field is small compared to the guide field. For example, this suggests that  $E_{\parallel}$  is the most important reconnection-driven heating mechanism in turbulent systems with  $\delta B/B \ll 1$ , consistent with the results of gyrokinetic simulations<sup>23</sup>. Notably, such reconnection is not likely to produce large fluxes of energetic particles. In reconnecting systems with broad current layers where the strength of the effective reconnecting magnetic field increases with time as stronger magnetic fields convect toward the reconnection site (as may be the case in a solar flaring current sheet)<sup>30</sup>, the rate of production of the most energetic electrons should increase rapidly with time.

A notable limitation of this study is the artificial ‘2D’ constraint (equivalent to  $\partial/\partial z = 0$ ). A recent study<sup>19</sup> showed that electron energization is greatly enhanced in a three-dimensional system with a strong guide field where reconnection becomes turbulent and high-energy electrons are able to move freely to sample regions where energy release is taking place. However, in three-dimensional systems with a weak guide field, transport is diminished and there is little enhancement (Dahlin et al., in preparation). This suggests that the most efficient energetic electron production might occur for  $b_g \sim 1$  where the Fermi mechanism and three-dimensional dynamics are both important. A complete theory of the production of energetic electrons from reconnection must incorporate the role of the guide field in transport and in the strength of the various energy drive mechanisms.



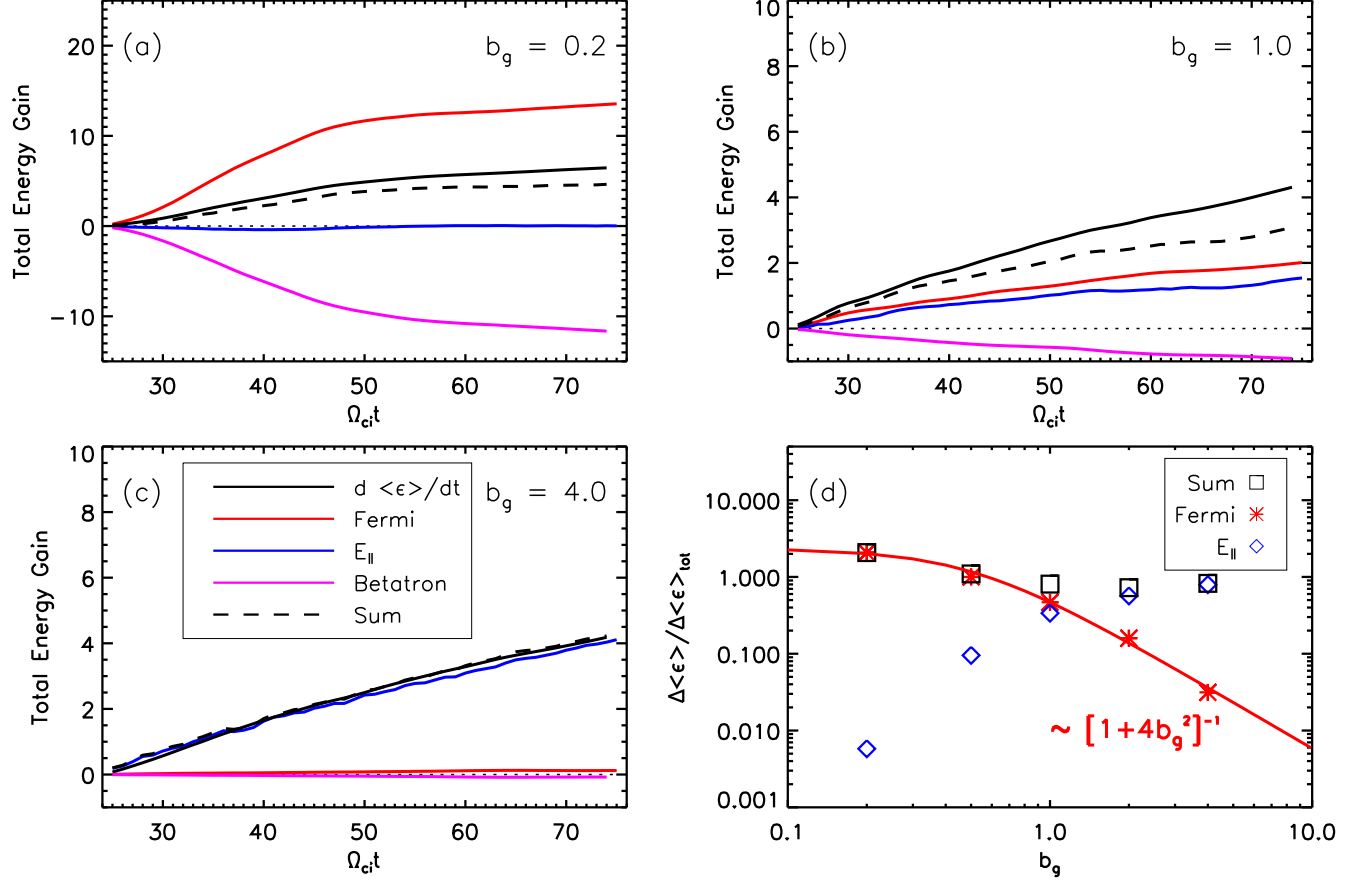


FIG. 1. (a)-(c) Cumulative electron heating due to Fermi reflection (red),  $E_{\parallel}$  (blue) and betatron acceleration (magenta) for three different values of  $b_g$ . (d) Total electron energy gain due to Fermi and  $E_{\parallel}$  as a function of guide field.

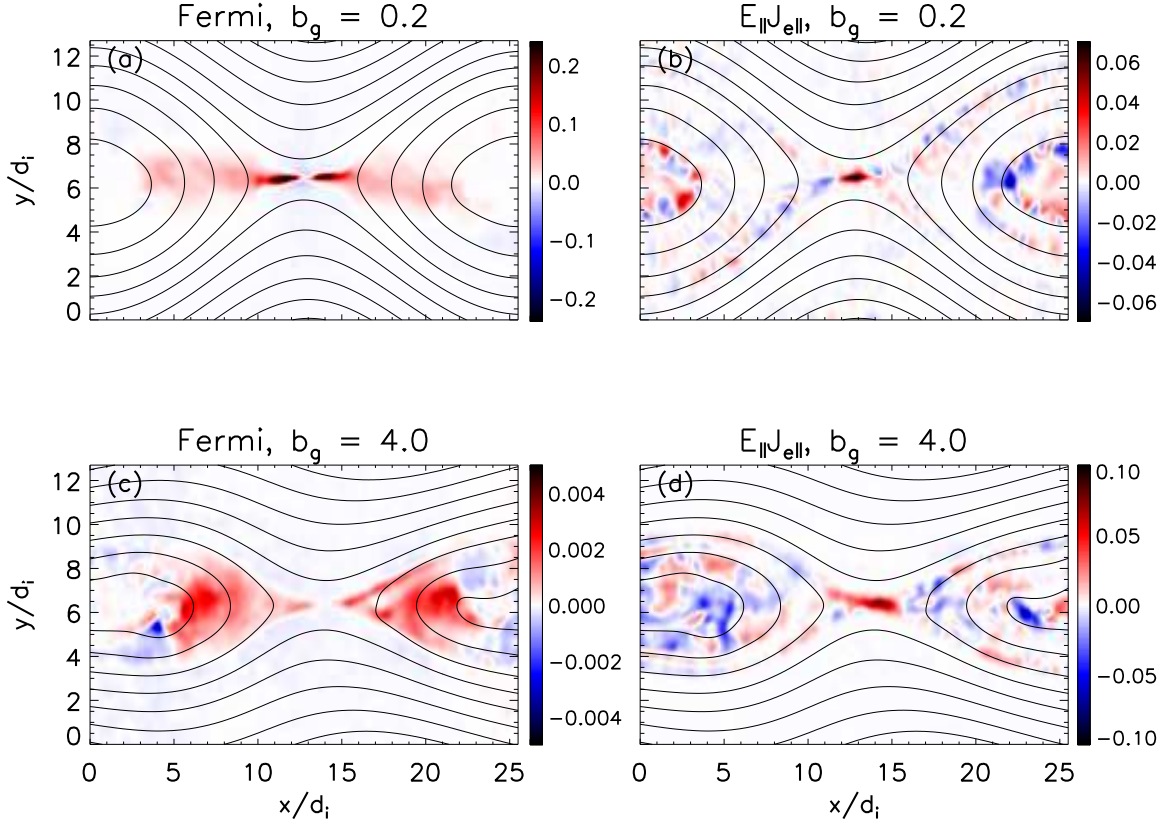


FIG. 2. (a)(c) Fermi acceleration for two values of the guide field. (b)(d)  $E_{\parallel} J_{e\parallel}$  acceleration for two values of the guide field, where  $J_{e\parallel}$  is the parallel component of the electron current.

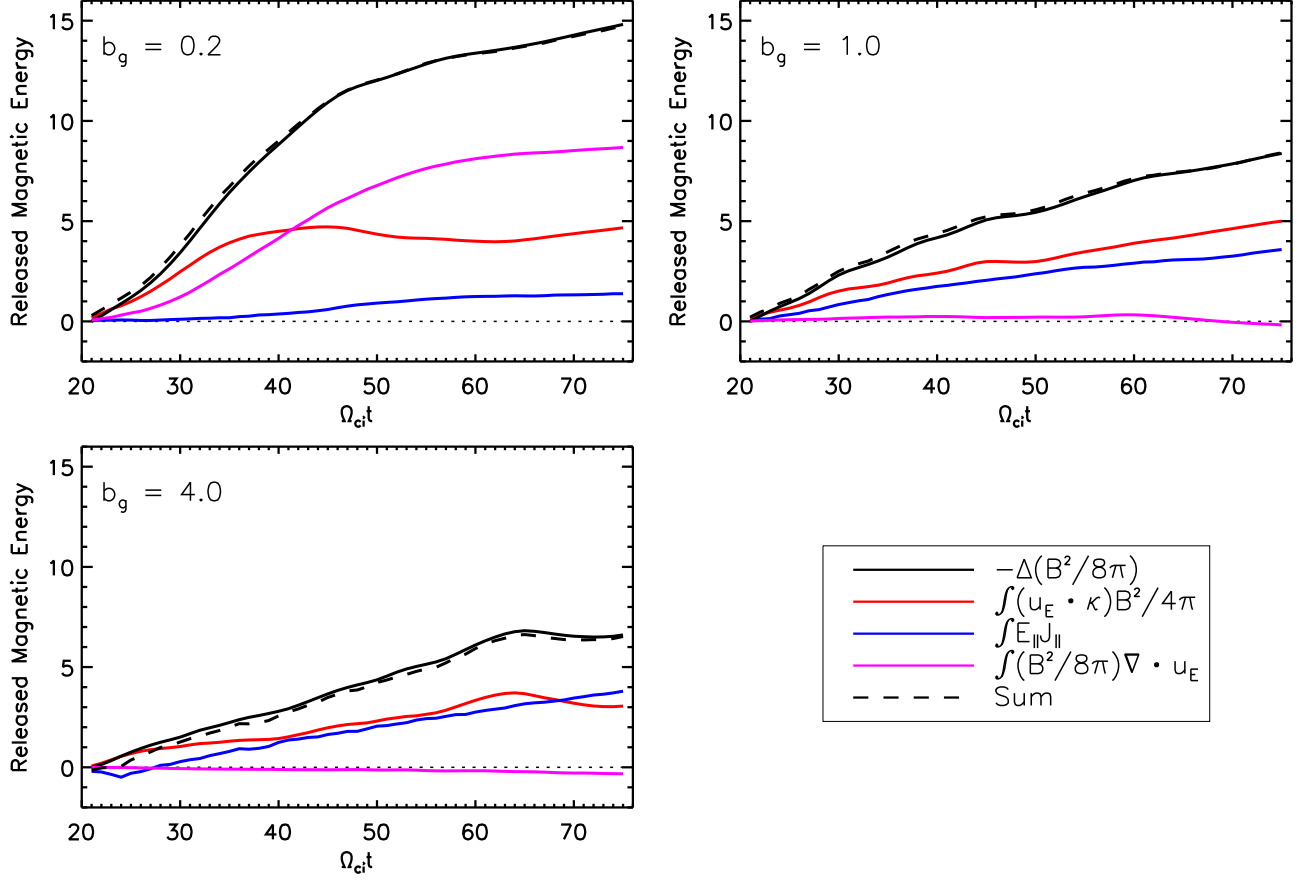


FIG. 3. Time dependence of the spatially integrated mechanisms for magnetic energy release given in Eq. 3 for guide fields  $b_g = 0.2, 1.0$  and  $4.0$ .

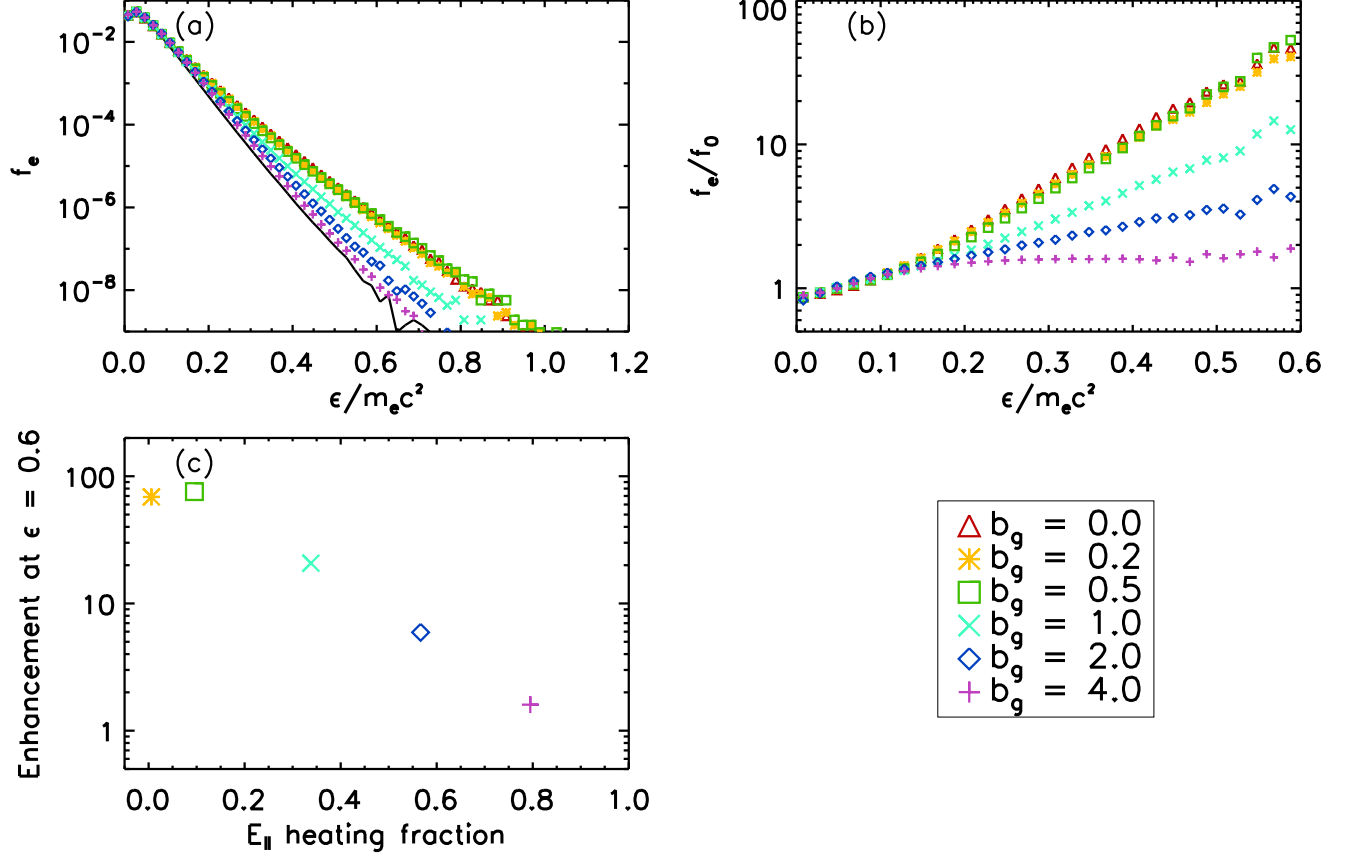


FIG. 4. (a) Electron energy spectra at  $\Omega_{ci}t = 75$ . (b) Enhancement relative to initial spectrum  $f_e(\epsilon, t = 75)/f_e(\epsilon, t = 0)$ . (c) Energetic electron enhancement ( $\epsilon = 0.6$ ) versus fraction of electron heating due to  $E_{\parallel}$ . The  $E_{\parallel}$  heating for  $b_g = 0$  is not calculated due to the poor applicability of the guiding-center model.

This work has been supported by NSF Grant PHY1500460 and NASA grants NNX14AC78G, NNX14AF42G, and DOE grant DEFG0293ER54197. J.T.D. acknowledges support from the NASA LWS Jack Eddy Fellowship administered by the University Corporation for Atmospheric Research in Boulder, Colorado. Simulations were carried out at the National Energy Research Scientific Computing Center.

- <sup>1</sup>G. Drenkhahn and H. C. Spruit, *Astronomy & Astrophysics* **391**, 1141 (2002).
- <sup>2</sup>F. C. Michel, *Ap. J.* **431**, 397 (1994).
- <sup>3</sup>R. P. Lin, S. Krucker, G. J. Hurford, D. M. Smith, H. S. Hudson, G. D. Holman, R. A. Schwartz, B. R. Dennis, G. H. Share, R. J. Murphy, A. G. Emslie, C. Johns-Krull, and N. Vilmer, *Ap. J.* **595**, L69 (2003).
- <sup>4</sup>M. Øieroset, R. P. Lin, T. D. Phan, D. E. Larson, and S. D. Bale, *Phys. Rev. Lett.* **89**, 195001 (2002).
- <sup>5</sup>S. Krucker, H. S. Hudson, L. Glesener, S. M. White, S. Masuda, J.-P. Wuelser, and R. P. Lin, *Ap. J.* **714**, 1108 (2010).
- <sup>6</sup>M. Oka, S. Ishikawa, P. Saint-Hilaire, S. Krucker, and R. P. Lin, *The Astrophysical Journal* **764**, 6 (2013).
- <sup>7</sup>M. Hoshino, T. Mukai, T. Terasawa, and I. Shinohara, *J. Geophys. Res.* **106**, 25,979 (2001).
- <sup>8</sup>S. Zenitani and M. Hoshino, *Ap. J. Lett.* **562**, L63 (2001).
- <sup>9</sup>J. F. Drake, M. A. Shay, W. Thongthai, and M. Swisdak, *Phys. Rev. Lett.* **94**, 095001 (2005).
- <sup>10</sup>P. L. Pritchett, *J. Geophys. Res.* **111**, A10212 (2006), 10.1029/2006JA011793.
- <sup>11</sup>J. Egedal, W. Daughton, J. F. Drake, N. Katz, and A. Lê, *Phys. Plasmas* **16**, 050701 (2009), 10.1063/1.3130732.
- <sup>12</sup>M. Oka, T.-D. Phan, S. Krucker, M. Fujimoto, and I. Shinohara, *Ap. J.* **714**, 915 (2010).
- <sup>13</sup>M. Hoshino, *Phys. Rev. Lett.* **108**, 135003 (2012).
- <sup>14</sup>Y. E. Litvinenko, *Ap. J.* **462**, 997 (1996).
- <sup>15</sup>J. Egedal, W. Daughton, and A. Lê, *Nature Phys.* **8**, 321 (2012).
- <sup>16</sup>J. F. Drake, M. Swisdak, H. Che, and M. A. Shay, *Nature* **443**, 553 (2006).
- <sup>17</sup>J. F. Drake, M. Opher, M. Swisdak, and J. N. Chamoun, *Ap. J.* **709**, 963 (2010).
- <sup>18</sup>J. F. Drake, M. Swisdak, and R. Fermo, *The Astrophysical Journal Letters* **763**, L5 (2013).
- <sup>19</sup>J. T. Dahlin, J. F. Drake, and M. Swisdak,

- Physics of Plasmas **22**, 100704 (2015), <http://dx.doi.org/10.1063/1.4933212>.
- <sup>20</sup>J. T. Dahlin, J. F. Drake, and M. Swisdak, Phys. Plasmas **21**, 092304 (2014).
- <sup>21</sup>F. Guo, H. Li, W. Daughton, and Y.-H. Liu, Phys. Rev. Lett. **113**, 155005 (2014).
- <sup>22</sup>X. Li, F. Guo, H. Li, and G. Li, The Astrophysical Journal Letters **811**, L24 (2015).
- <sup>23</sup>R. Numata and N. F. Loureiro, Journal of Plasma Physics **81**, 305810201 (17 pages) (2015).
- <sup>24</sup>H. Wang, Q. Lu, C. Huang, and S. Wang, The Astrophysical Journal **821**, 84 (2016).
- <sup>25</sup>T. G. Northrop, Reviews of Geophysics **1**, 283 (1963).
- <sup>26</sup>A. Beresnyak and H. Li, The Astrophysical Journal **819**, 90 (2016).
- <sup>27</sup>A. Zeiler, D. Biskamp, J. F. Drake, B. N. Rogers, M. A. Shay, and M. Scholer, J. Geophys. Res. **107**, 1230 (2002).
- <sup>28</sup>N. A. Bobrova, S. V. Bulanov, J. I. Sakai, and D. Sugiyama, Physics of Plasmas **8** (2001).
- <sup>29</sup>Y. Lin, L. C. Lee, and C. F. Kennel, Geophysical Research Letters **19**, 229 (1992).
- <sup>30</sup>J. F. Drake and M. Swisdak, Physics of Plasmas **21**, 072903 (2014), <http://dx.doi.org/10.1063/1.4889871>